

Milliarcsec-scale polarisation observations of the gravitational lens B1422+231

A.R. Patnaik¹, A.J. Kembell², R.W. Porcas¹, M.A. Garrett³

¹*Max-Planck-Institut für Radioastronomie, Auf dem Hügel 69, D-53121 Bonn, FRG*

²*National Radio Astronomy Observatory, PO Box 0, Socorro, NM 87801, USA*

³*Joint Institute for VLBI in Europe, Postbus 2, 7900 AA Dwingeloo, The Netherlands*

ABSTRACT

We present polarisation observations of the gravitational lens system B1422+231 made at 8.4 GHz using the VLBA and the 100m telescope at Effelsberg. All four images of the quasar show structure on the milliarcsec scale. The three bright images show tangential stretching as expected from lens models. Some basic properties of gravitational lensing are exhibited by this system. The surface brightness of images A and B are the same and the parity reversal expected in image B is revealed, for the first time, by polarisation observations. There is a large differential Faraday rotation between images A and B.

Key words: gravitational lensing

1 INTRODUCTION

Radio polarisation observations can be used as a powerful tool in the study of gravitational lenses. Such observations yield two useful parameters - the distributions of polarised intensity (or degree of polarisation) and of position angle (PA) of polarisation. Both the degree and PA of polarisation of a point in an object are unchanged in its images by the action of a gravitational lens. In gravitational lens searches the equal degrees of polarisation of images can be used to discriminate amongst lens candidates. However, the measured PAs of polarisation need not be the same at any given frequency, since the different ray paths of the images can undergo different amounts of Faraday rotation. After correcting for the rotation measure (RM), the intrinsic PA (PA at zero wavelength) must be the same for the lensed images.

Any difference in RM between lensed images can give clues to the nature of the lensing galaxy. For a gas-rich lens or a spiral galaxy lens, the RMs of each lensed image (and also their difference) are expected to be large compared to those from an elliptical galaxy lens. The difference in RMs is assumed to be caused by the interstellar medium of the lens.

The polarisation angle is not altered by the gravitational deflection even though the total intensity (Stokes parameter I) distribution can be distorted (Dyer & Shaver 1992). Milliarcsec-scale observations of the gravitational lens B0218+357 have been used to demonstrate this feature of the gravitational potential (Patnaik, Porcas & Browne

1995). This property can help identify corresponding features in distorted lensed images, even when this is unclear from total intensity maps, since their degrees of polarisation must be equal, and their PAs of polarisation must be parallel (after correction for any differential RM).

The gravitational lens system B1422+231 was discovered by Patnaik et al. (1992); it is a 4-image system with maximum image separation of 1.3 arcsec (Fig. 1). The background radio source is associated with a 15.5 mag quasar at a redshift of 3.62. The lensing galaxy has a redshift of 0.338 (Kundić et al. 1997, Tonry 1998). The lensed images have similar spectra at radio as well as optical wavelengths. The three bright images, A, B and C, have similar radio polarisation properties; image D is too weak at radio wavelengths for its polarisation properties to be determined reliably. The source has been observed in IR and optical bands (Lawrence et al. 1992; Remy et al. 1993; Yee & Ellingson 1994, Bechtold & Yee 1995; Akujor et al. 1996; Yee & Bechtold 1996; Impey et al. 1996) and models of the lensed system have been proposed by several authors (Hogg & Blandford 1994; Narasimha & Patnaik 1994, Kormann, Schneider & Bartlemann 1994; Mao & Schneider 1998).

In this paper we describe high resolution radio polarisation observations of the gravitational lens B1422+231, made at 8.4 GHz using the VLBA together with the Effelsberg radio telescope. The observations and data reductions are described in Section 2; the results and their implications are discussed in Section 3.

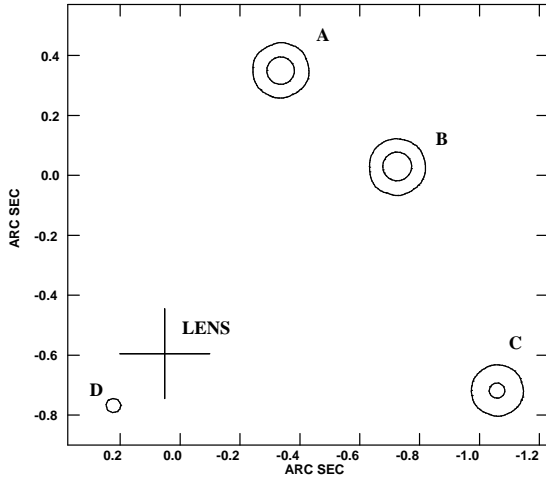


Figure 1. Location of lensed images (in circles) and the lensing galaxy (marked +) in B1422+231.

2 OBSERVATIONS AND ANALYSIS

We observed B1422+231 on 1997 June 11/12 at 8.4 GHz, using all 10 antennas of the VLBA and the 100m telescope at Effelsberg. We recorded eight 8 MHz channels using a dual polarisation set-up, giving a total bandwidth of 32 MHz in each polarisation; we used 1-bit sampling of the signals. The data were correlated at a single field centre using the VLBA correlator. The sampling in time was 1 sec and in frequency 0.5 MHz. Since the image separations are large (the largest is 1.3 arcsec) compared to the synthesised beam (about 1 milliarcsec), it is important to preserve short time and frequency sampling in the analysis, as this avoids smearing of the visibility function, and hence distortion of the images near the edge of the field.

We observed in cycles consisting of 6 mins. on the calibration source 1308+326 and 16 mins. on B1422+231, resulting in a total integration time on B1422+231 of 410 minutes. In between we observed the calibrator sources 1226+023 (3C 273), 1749+096 and 1823+568 once each for 8 min.

The data were analysed using the NRAO software package AIPS. The data were corrected for the parallactic angle variations of the telescopes, and amplitude calibrations determined from the measured system temperatures and gains were applied. The phase slopes across the 8 MHz bands were aligned using the pulse-cal information from each telescope. Standard fringe-fitting was then performed on the calibration sources. After careful editing, we used the data on 1308+326 and 1823+568 to determine the bandpass function.

We used the following procedures to determine the instrumental polarisation terms and correct for them. After applying the total intensity calibration table, we fringe-fit the cross-hand (RL, LR) data of 1308+326 on the single baseline Los Alamos (our reference antenna) to Pie Town. In this way one determines the residual LHC-RHC delay offset for the reference antenna. The solutions were smoothed, copied to the calibration table and applied to the main data.

Since the sources used for polarisation calibration usually have structures at milliarcsec-scales, a model of the

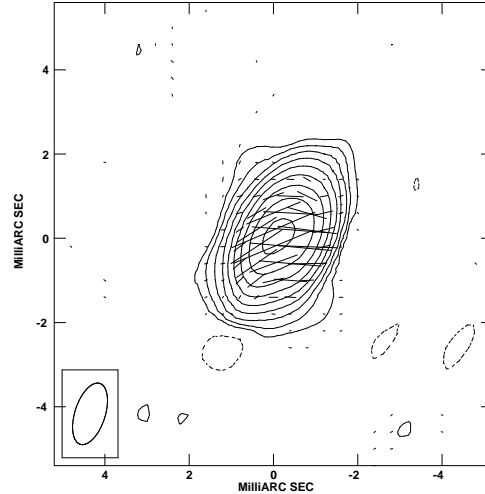


Figure 2. 8.4 GHz map of 1308+326 with polarisation overlaid as vectors proportional to the polarised intensity. The contour levels are $-2, -1, 1, 2, 4, 8, 16, 32, 64, 128 \times$ the contour interval which is chosen as the 3σ noise in the map. The contour interval is $4.83 \text{ mJy beam}^{-1}$ and the peak in the map is $1.514 \text{ Jy beam}^{-1}$. The integrated flux density is 2.648 Jy . The convolving beam of $1.52 \times 0.72 \text{ mas}$ in position angle -17.8° is drawn at the lower left-hand corner of the map.

source is required in order to determine the instrumental polarisation leakage terms. 1308+326 was mapped to determine its structure and the model was used in the AIPS task LPCAL. 1308+326 had a peak polarisation of 3.6 percent, and typical instrumental polarisation terms were 1 to 2 percent for the VLBA telescopes and 4 percent for Effelsberg.

We have not been able to determine the absolute angle of polarisation. In Fig. 2 we show the map of 1308+326 with electric vectors overlaid on the total intensity contours; the length of the vector is proportional to polarised intensity. The PA of polarisation changes within the source, but from the integrated flux density of Q and U Stokes parameters we find that the PA of 1308+326 was 11° . We do not have polarisation PA measurements of 1308+326 sufficiently close to our observing epoch to calibrate the absolute angle of polarisation.

After performing the above polarisation calibration procedures, the data for B1422+231 were analysed. Fringe-fitting sources with widely separated components, such as B1422+231, can prove difficult, especially if no component consistently dominates on all baselines (see Porcas, 1994). This is often the case for gravitational lenses, since the equal surface brightness property of lensed images tends to result in roughly equal contributions from them for baselines on which they are resolved. The AIPS fringe-fitting task FRING can utilise a source model, and this feature can be used to guide the process.

We used the following procedure for the B1422+231 data. First the data are fringe-fitted using a point source model, and after applying the solutions, a map is made using the AIPS tasks IMAGR and CALIB. Since the lensed images are widely separated, we map each image in a separate sub-field. Even though this map is inaccurate, the images can be identified at their correct locations. A second fringe-fit is then made, using a model comprising components from each of the images, and a new map made. This process is

Image	Total flux density in mJy	Polarised intensity in mJy	Deconvolved size in mas×mas, PA	ΔRA_1 in mas	ΔDec_1 in mas	ΔRA_2 in mas	ΔDec_2 in mas
A	152±2	3.7	2.11×0.37, 53°	389.25	319.98	389.29	320.00
B	164±2	2.9	2.52×0.28, 43°	0	0	0	0
C	81±1	0.95	1.57×0.45, 16°	-333.88	-747.71	-333.86	-747.71
D	5±0.5		0.89×0.59, 123°	950.65	-802.15	950.67	-802.12

Table 1. Total and polarisation flux densities and deconvolved sizes of the lensed images of B1422+231. Flux densities are given in mJy, and the deconvolved sizes are given in terms of major and minor axes (in mas) of the fitted elliptical gaussian and the PA (in degrees) of the major axis. Polarisation flux is the sum over the image area. The image separations are given in mas with respect to image B: the columns (5 and 6) with subscript 1 have been determined by JMFIT which fits an elliptical gaussian to the entire image and the columns (7 and 8) with subscript 2 have been determined by MAXFIT which fits a quadratic to the peak in the image.

repeated a few times to converge on a consistent fringe-fit solution.

For the final map of the 4 image subfields, several cycles of phase self-calibration were performed. Polarisation maps were made using usual procedures.

3 RESULTS AND DISCUSSION

Our maps of the 4 images of B1422+231, made using uniform weighting, are shown in Figures 3 and 4. The two strongest images, A and B, have highly elongated structures, confirming the basic image shapes derived from VLBA 15 GHz observations by Patnaik and Porcas (1998). There is only a single peak in the total intensity distributions of the images, so we fit a single elliptical Gaussian function to each image using task JMFIT. The 3 strongest images are many resolution elements in length, and the fits are not particularly good, but they do parameterize some basic image properties. The total flux densities (column 2), polarised intensity (column 3), deconvolved sizes (column 4) and relative positions (columns 5 and 6) are listed in Table 1. As the strongest images are highly elongated, we have also made estimates of the (local) positions of the central peaks using MAXFIT (columns 7 and 8 in Table 1). However, there is no obvious compact feature within the smooth image structures, and the peak positions are thus not well defined, especially in the direction of elongation of the images. We therefore estimate an uncertainty in defining the image positions of about 1/20th of the image size in the corresponding direction.

Kochanek, Kolatt & Bartelmann (1996) have suggested that repeated measurements with $\sim 10\mu\text{arcsec}$ precision of the separation between highly magnified image pairs such as A and B, would yield a measurement of the proper motion of the lens with respect to the observer. Movement of the lens can result in a detectable image motion due to magnification along the tangential direction. The B1422+231 system may prove difficult to use for such proper motion studies, since the elongation of the relatively featureless images results in an increased position uncertainty in the same direction. This may also apply to the bright ‘merging image’ pairs of other 4-image gravitational lens systems if they do not contain highly compact features.

None of the images exhibits an obvious asymmetric structure of the canonical “core-jet” type in its total intensity distribution. Whilst such morphologies occur frequently

amongst radio-loud quasars, it should be noted that the radio spectrum of B1422+231 is peaked around 5 GHz, and the relatively steep spectrum at higher frequencies (Patnaik et al. 1992, Patnaik et al. 1999, in preparation) does not show any evidence for “core dominance”. In any case, the magnification and distortion of the background source structure by the lens must also be taken into account. Images A and B are highly magnified, and image C is magnified by a factor of a few in most lens models. Without the presence of the lens, B1422+231 would most likely be a 19 mag quasar with a radio flux density at 8.4 GHz of only ca 20 mJy - almost a “radio quiet” quasar.

We obtain a number of important results from the total intensity distribution. We have investigated the surface brightness of the 2 strongest images, A and B, by measuring the flux in each image contained above the contour level of 1 mJy beam⁻¹. The flux ratio of 0.94 ± 0.02 is essentially the same as the area ratio of 0.95 ± 0.05 , thus demonstrating that the surface brightness is the same in these two lensed images. This accords with the property that gravitational lensing does not change the surface brightness of an image.

A second result is that the PA of elongation of the structures of A, B and C are tangential with respect to the lens, which is believed to be located close to image D (Fig. 1). This is expected from lens models where the background source lies close to the diamond caustic. Even though image D is weak, it is interesting to note that its elongation appears ‘radial’ with respect to the lens.

The polarisation distribution in the images is more remarkable. Although we do not have enough sensitivity to detect polarised emission from the weak D image, the polarisation distribution in the other 3 images is clearly non-uniform, and the PA of polarisation changes over the images. In particular, there is a “reflection symmetry” between A and B in the polarisation distribution along the image major axes. The SW of A and NE of B are regions of little or no polarisation. Progressing from these points along the image axes, the degree of polarisation rises to $\sim 2.5\%$ at the central peaks, with polarisation angles of -23° in A and -43° in B. Progressing further, the PAs rotate to final values of 40° in the NE of A, and 22° in the SW of B.

Since the polarisation properties of the source are not changed by gravitational lensing, we may use such matching features in these images to identify corresponding regions. Thus the run of polarisation emission in opposite directions in A and B reveals the opposite orientation of these images

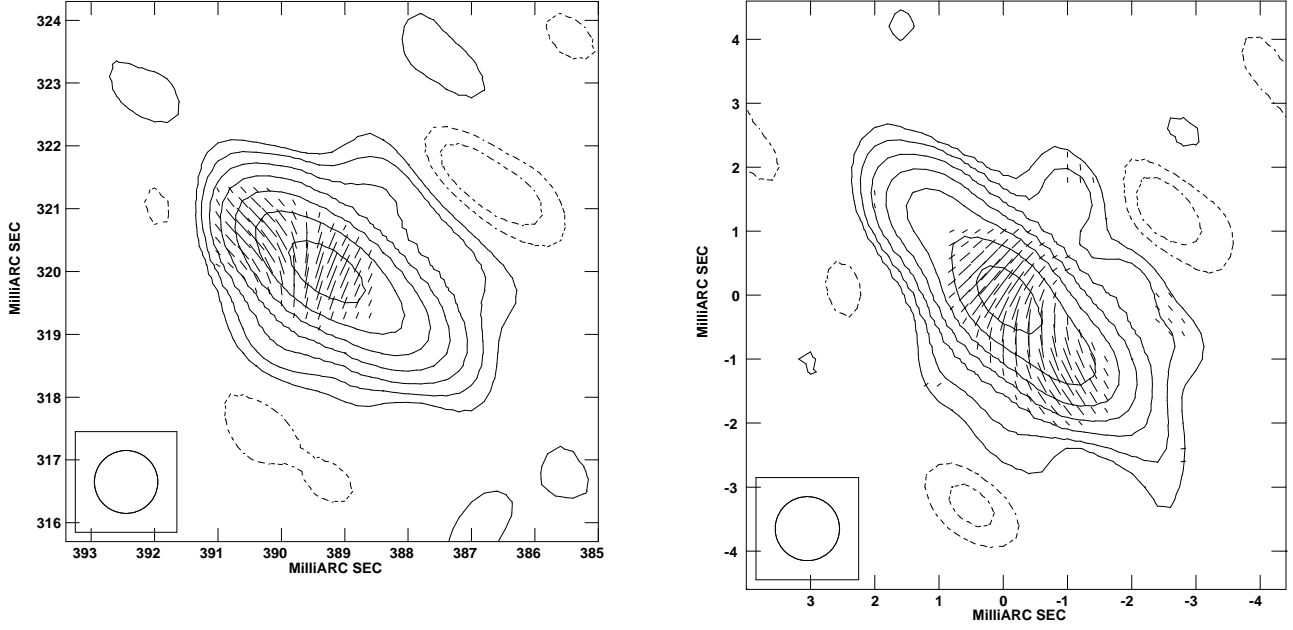


Figure 3. 8.4 GHz map of B1422+231 A (left) and B (right). The contour levels for all the images are $-2, -1, 1, 2, 4, 8, 16, 32, 64, 128 \times$ the contour interval which is chosen as the 3σ noise in the map. For image A, contour interval is $0.72 \text{ mJy beam}^{-1}$ and peak flux density is $62.9 \text{ mJy beam}^{-1}$ and for image B contour interval is $0.72 \text{ mJy beam}^{-1}$ and the peak is $64.6 \text{ mJy beam}^{-1}$. The convolving beam of 1 mas circular gaussian is drawn at the lower left-hand corner in each map. Polarisation is plotted as electric vectors proportional to the polarised intensity.

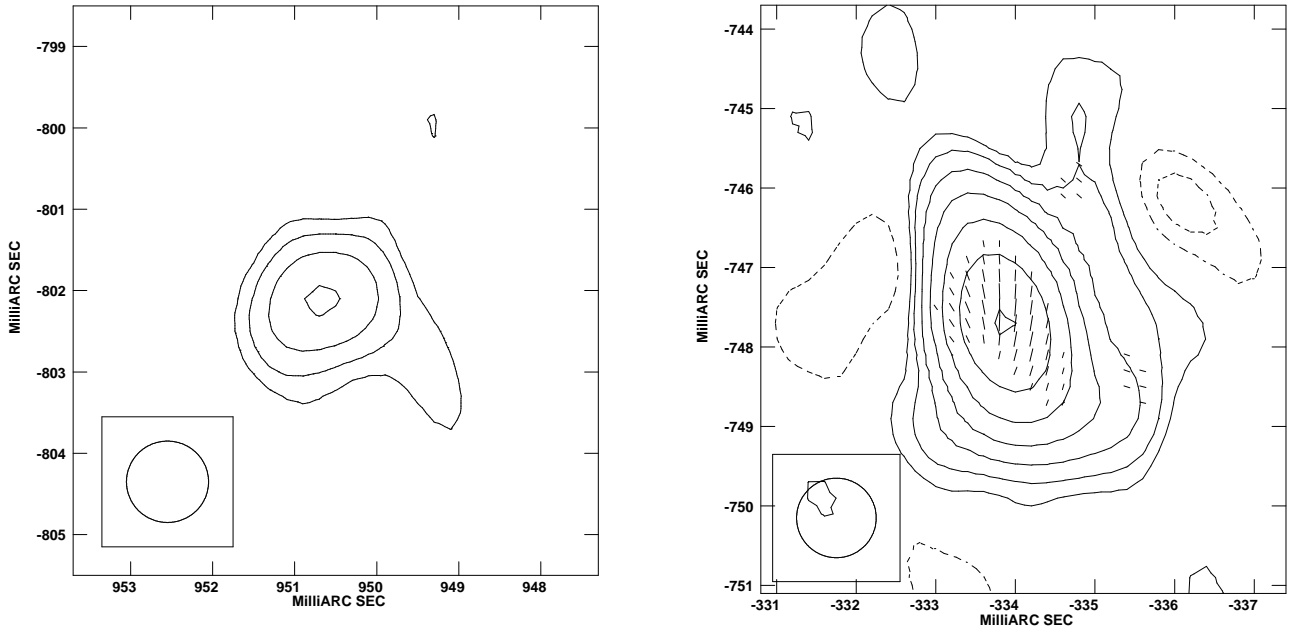


Figure 4. 8.4 GHz map of B1422+231 C (right) and D (left). For image C, the contour interval is $0.62 \text{ mJy beam}^{-1}$ and the peak flux density is $41.8 \text{ mJy beam}^{-1}$. For image D, the contour interval is $0.36 \text{ mJy beam}^{-1}$ and the peak flux density is $3.1 \text{ mJy beam}^{-1}$. The convolving beam of 1 mas circular gaussian is drawn at the lower left-hand corner in each map. Polarisation is plotted as electric vectors proportional to the polarised intensity.

in the tangential direction. This is entirely expected, since these two bright images must have opposite parity. Indeed, the slight Southerly offset of the polarisation peaks (in the NE of A and SW of B) from the axis of the total intensity distributions establishes their opposite parity directly. Even

though the polarisation of C is weak, the change of polarisation within the image matches closely with that of image A; this is expected as A and C should have the same parity.

From the measurements made on the images, noted above, it is clear that there is a systematic difference of 20°

between the polarisation PAs of corresponding features in A and B. Since the gravitational action of the lens does not change the polarisation angle of regions of the object in either image, we attribute this observed difference to Faraday rotation along one or both image paths; the difference in RM amounts to $280 \pm 20 \text{ rad m}^{-2}$. Images A and B are considered to be "merging images" and hence their ray paths, separated by 0.5 arcsec and located on the same side of the lens, are expected to traverse similar environments in the lens. Moreover, these images are located some distance, (ca 1 arcsec) from the lens centre. The differential RM is assumed to be caused by the magneto-ionic medium of the lens. Such high RMs are generally found in gas-rich environments; thus it is rather surprising that this lens, thought to be an elliptical galaxy, can give rise to this large differential Faraday rotation.

VLBI measurements of lensed image structures can potentially provide more constraints for lens modelling than image relative flux densities and positions. These are conveniently presented by the relative magnification matrix between image pairs. Ideally there would be at least 3 non-collinear points in the source, recognisable in each image; the matrix could then be determined by considering the transformation of 2 non-parallel vectors.

In B1422+231 there is only a single peak in the total intensity distribution, but there are separate and distinct peaks in the polarised flux distributions of A and B, which we recognise as corresponding points from their polarisation properties. We measured the positions of these peaks in the maps of the A and B images and attempted to determine an A/B relative magnification matrix. However, we were unable to get values for the matrix elements consistent with the relative flux densities of the images. The elements derived by this method are in any case ill-defined, because the three peaks used are almost collinear.

We have used the separations between the polarisation peaks within the A and B images to test the matrices given by Hogg & Blandford (1992). Our measured separation in B is 1.478 mas in PA -145.2° . Using their two matrices, we find that this transforms to a predicted separation in image A of 1.607 mas in PA 27.9° , and 1.680 mas in PA 22.8° respectively. The measured separation is 1.0 mas in PA 62.6° . It is perhaps not surprising that these models fail in their predictions, as they are based on an measured optical flux ratio between A and B of 0.77. Transformation matrices are not explicitly given for the other models, and so we have not tested them. However, all the models predict tangential stretching of the three bright images.

4 CONCLUSION

We have presented polarisation observations of the gravitational lens system B1422+231 made using the VLBA and Effelsberg at 8.4 GHz. Our 1 mas resolution maps of the images reveal the parity reversal of image B through the distribution of polarised emission. We show that the surface brightness is the same in A and B, as expected from preservation of the source surface brightness. We find that the differential Faraday rotation between A and B is rather large, considering that the lens is an elliptical galaxy. It is difficult to derive a relative magnification matrix from the

total intensity and polarisation distributions of the A and B images. Published matrices, however, do not successfully predict the structural relationships between A and B.

ACKNOWLEDGMENTS

We thank D. Narasimha for helpful discussion and J. Schmid-Burgk for critical comments. The National Radio Astronomy Observatory is a facility of the National Science Foundation operated under cooperative agreement by Associated Universities, Inc.

REFERENCES

- Akujor, C.E., Patnaik, A.R., Smoker, J.V., Garrington, S.T., 1996, in Kochanek, C.S, Hewitt, J.N., eds, Proceedings of the 173rd Symposium of the IAU 'Astrophysical applications of gravitational lensing', Kluwer Academic Publishers, Dordrecht, p335
- Bechtold, J., Yee, H.K.C., 1995, AJ, 110, 1984
- Dyer, C.C., Shaver, E.G., 1992, ApJ, 390, L5
- Hogg, D.W., Blandford, R.D., 1994, MNRAS, 268, 889
- Impey, C.D., Foltz, C.B., Petry, C.E., Browne, I.W.A., Patnaik, A.R., 1996, ApJ, 462, L53
- Kochanek, C.S., Kolatt, T.S., Bartelmann, M., 1996, ApJ, 473, 610
- Kormann, R., Schneider, P., Bartelmann, M., 1994, AA, 286, 357
- Kundić, T., Hogg, D.W., Blandford, R.D., Cohen, J.G., Lubin, L.M., Larkin, J.E., 1997, AJ, 114, 2276
- Lawrence, C.R., Neugebauer, G., Weir, N., Matthews, K., Patnaik, A.R., 1992, MNRAS, 259, 5P
- Mao, S., Schneider, P., 1998, MNRAS, 295, 587
- Narasimha, D., Patnaik, A.R., 1994, in Surdej, J., Fraipont-Caro, D, Grosset, E., Refsdal, S., Remy, M., eds, Proc. 31st Liège International Astrophysical Colloq., Gravitational Lenses in the Universe, Université de Liège, Belgique, p.295
- Patnaik, A.R., Browne, I.W.A., Walsh, D., Chaffee, F.H., Foltz, C.B., 1992, MNRAS, 259, 1P
- Patnaik, A.R., Porcas, R.W., 1998, in Zensus, J.A., Taylor, G.B., Wrobel, J.M., eds, Radio Emission from Galactic and Extragalactic Compact Sources, ASP Conference Series, Volume 144, IAU Colloquium 164, p319
- Patnaik, A.R., Porcas, R.W., Browne, I.W.A., 1995, MNRAS, 274, L5
- Porcas, R.W., 1994, in Zensus, J.A., Kellermann, K.I., eds, 'Compact Extragalactic Radio Sources', NRAO, p125
- Remy, M., Surdej, J., Smette, A., Claeskens, J.-F., 1993, AA, 278, L19
- Tonry, J.L., 1998, AJ, 115, 1
- Yee, H.K.C., Bechtold, J., 1996, AJ, 111, 1007
- Yee, H.K.C., Ellingson, E., 1994, AJ, 107, 28

This paper has been produced using the Royal Astronomical Society/Blackwell Science \LaTeX style file.